Water-induced convection in the Earth's mantle transition zone

Guillaume C. Richard[1] and David Bercovici[2]

[1]   Water enters the Earth's mantle by subduction of oceanic lithosphere. Most of this water immediately returns to the atmosphere through arc volcanism, but a part of it is expected as deep as the mantle transition zone (410–660 km depth). There, slabs can be deflected and linger before sinking into the lower mantle. Because it lowers the density and viscosity of the transition zone minerals (i.e., wadsleyite and ringwoodite), water is likely to affect the dynamics of the transition zone mantle overlying stagnant slabs. The consequences of water exchange between a floating slab and the transition zone are investigated. In particular, we focus on the possible onset of small-scale convection despite the adverse thermal gradient (i.e., mantle is cooled from below by the slab). The competition between thermal and hydrous effects on the density and thus on the convective stability of the top layer of the slab is examined numerically, including water-dependent density and viscosity and temperature-dependent water solubility. For plausible initial water content in a slab (≥ 0.5 wt %), an episode of convection is likely to occur after a relatively short time delay (5–20 Ma) after the slab enters the transition zone. However, water induced rheological weakening is seen to be a controlling parameter for the onset time of convection. Moreover, small-scale convection above a stagnant slab greatly enhances the rate of slab dehydration. Small-scale convection also facilitates heating of the slab, which in itself may prolong the residence time of the slab in the transition zone.
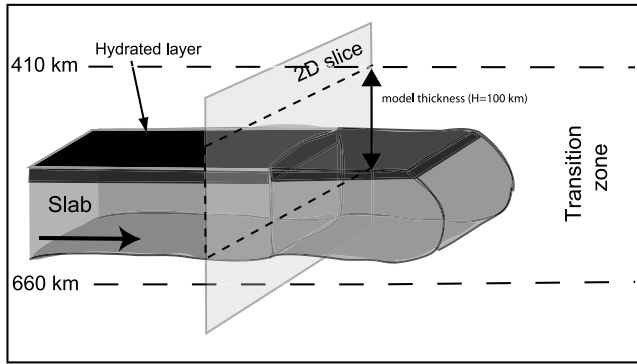
1.   Introduction

[2]   Water can be stored as hydrogen ions in the nominally anhydrous minerals composing the Earth's mantle [*Thompson*, 1992; *Bell and Rossman*, 1992; *Kohlstedt et al.*, 1996] and has a remarkable ability to affect some of their key physical and chemical properties such as rheology and melting behavior [*Hirth and Kohlstedt*, 1996; *Mei and Kohlstedt*, 2000]. To better constrain the water distribution within the Earth's mantle it is important to consider the subduction "entry point" of the Earth's so-called deep water cycle [*Jacobsen and van der Lee*, 2006]. The oceanic crust and shallow lithosphere undergo lengthy traverses along the bottom of the oceans and are thus well hydrated when they start to subduct. During early subduction a large part of the subducted water is released back to the hydrosphere through arc volcanism, but in cold slabs a significant amount (up to 40% of its initial water content) is released by the breakdown of sediments, crust, and serpentinized mantle at high pressure and temperature [*Ruepke et al.*, 2004] after which it is likely stored in various dense hydrous magnesium-silicate phases (DHMS). These phases can be carried to depths of 450 km [*Ohtani et al.*, 2004; *Schmidt and Poli*, 1998] where high-pressure olivine polymorphs (wadsleyite, ringwoodite) can retain water [*Komabayashi et al.*, 2005].

[3]   Two phenomena make the transition zone (410–660 km depth) an ideal region for slabs to dehydrate. First, the water solubility of the primary minerals composing this layer is very high (up to 2.4 wt % in ringwoodite and up to 2.7 wt % in wadsleyite) [*Kohlstedt et al.*, 1996]. Second, the transit time of a slab in this layer can be very long (tomographic imaging depicts many slabs horizontally deflected and remaining stagnant in the transition zone [*Zhao*, 2004]). The dehydration of slabs directly entering the lower mantle has been studied previously [*Richard et al.*, 2007]. Three processes can be involved in slab dehydration and return of water to the mantle: (1) The stability of the hydrated minerals (at this depth the relevant minerals are, in addition to the wet olivine polymorphs mentioned above, the DHMS; moreover, proposed phase diagrams [*Komabayashi et al.*, 2004] locate the main dehydration processes at the base of the transition zone (660 km) or lower); (2) the solid-state diffusion of water from the wet slab into the drier surrounding mantle (in a previous study [*Richard et al.*, 2006], we demonstrated that the diffusive water flux out of the slab is very weakly dependent on the temperature dependence of the solubility and that given typical residence times of slabs floating horizontally across the transition zone (50 Ma or longer) essentially 50–100%

[1]Earth Sciences Institute, J. W. Goethe University, Frankfurt am Main, Germany.
[2]Department of Geology and Geophysics, Yale University, New Haven, Connecticut, USA.

Figure 1. Water-induced convection at the top of a stagnant slab. The essence of the model hypothesis: The lowering of density and viscosity by water allows for the onset of small-scale convection in the direction perpendicular to the slab motion.

of the water brought into the transition zone is expelled into the transition zone); and (3) the advection of a water-bearing matrix by small-scale convective transport can circulate water through the mantle.

[4] Water-related convective instability has already been proposed to be active by advection of water from a putative melt layer on the top of the transition zone [*Leahy and Bercovici*, 2007] and to be triggered by the different stages (mantle wedge, transition zone) of dehydration of a subducting lithosphere [*Gerya and Yuen*, 2003]. Here we focus on deeper slab dehydration into the transition zone as stated in scenario 3. The dynamics of a cool, wet and horizontally migrating slab in the transition zone is investigated using a two dimensional numerical model including the effects of the dissolved water on the density and viscosity of a stagnant slab. The mantle overlying the slab is cooled from below, i.e., the thermal gradient is reversed in comparison with the gradient in the longstanding problem of small-scale convection under oceanic lithosphere [*Richter and Parsons*, 1975; *Korenaga and Jordan*, 2003]. Given this thermally adverse but chemically favorable (hydration from below) condition for convective transport, we explore the control of the major parameters (water concentration, rheology, temperature) on the onset of gravitational instabilities (or wet diapirs). Our goal is to understand how water is recycled to the mantle. The consequences of this convective transport on stagnant slab dehydration process is then discussed.

2. Model, Constitutive Equations, and Numerical Methods

[5] Slabs that linger at the base of the transition zone are both cold and wet and thus induce two buoyant driving forces with opposite directions: A thermal density gradient pointing upward (from cold heavy slab to warm light mantle) which is dynamically stable, and simultaneously an unstable chemical (water-controlled) density gradient (from wet light slab to dry heavy mantle). Since the slab is cooling and dehydrating, these gradients are subject to change with time and control the onset time of convection (see section 4.1).

[6] The variables of interest are the water (hydrogen) content H and the temperature T. Initially, the slab is

essentially defined as a cold layer of viscous material underlying a warmer layer of mantle (Figure 1) and the top section of the slab (5 km thick) is uniformly hydrated (this homogeneous hydration is likely in plans orthogonal to the slab motion but not necessarily in the direction of the slab). The initial fields (Temperature and water concentration) are subject to random numerical perturbations (with the maximum amplitude of 10^{-14} (degree and ppm, respectively)). Recent studies [*Solomatov and Barr*, 2007] suggest that for Newtonian rheology cases, the effect of initial temperature perturbations on the onset of convection in normal settings (cooling from above) is limited. Similarly (see equation (7)), in our settings, effect of initial water concentration perturbations on the onset of convection are expected to be limited. All other properties (solubility, viscosity, density) are only water- and/or temperature-dependent; that is, compositional heterogeneities other than water are not taken into account. The problem is expected to be essentially two-dimensional because convection cells tend to align themselves in parallel with the direction of slab motion to minimize the interference with the background flow. Thus gradients of the variables of interest in the slab motion direction (y axis) are assumed to be negligible relative to gradients in x and z. Thermal convection (with infinite Prandtl number) is studied in a plane layer perpendicular to the direction of and fixed to the slab and including both the upper half of the slab (50 km thick) and the entire transition zone mantle above it (also 50 km thick, see Figure 1). Considering the very low value of the dissipation number ($Di = Lg\alpha/C_p \approx 10^{-7}$, where $L = 55$ km is the thickness of the convecting layer and $C_p = 1200$ J kg^{-1}K^{-1} the wadsleyite specific heat at constant pressure), we can use the Boussinesq approximation [*Schmeling*, 1989].

[7] The model can be described by the conservation equations for mass, momentum, energy, and water:

$$\nabla \cdot \mathbf{u} = 0 \tag{1}$$

$$-\nabla p + \nabla \cdot \underline{\tau} = \rho \mathbf{g} \tag{2}$$

$$\frac{\partial T}{\partial t} + \mathbf{u} \cdot \nabla T = \nabla \cdot (\kappa \nabla T) \tag{3}$$

where $\mathbf{u}$ denotes the velocity vector, p is pressure, $\mathbf{g}$ is gravity, T is temperature, and κ is thermal diffusivity.

[8] The transport of water is described using a potential formulation [*Richard et al.*, 2002] with which we take into account the temperature dependence of the water solubility:

$$\frac{\partial H}{\partial t} + \mathbf{u} \cdot \nabla H = \kappa_H \nabla \cdot \left(H^* \nabla \frac{H}{H^*} \right)$$
$$= \kappa_H \nabla^2 H + \kappa_H \nabla \cdot \left(H \nabla \frac{\mu_0}{RT} \right) \tag{4}$$

where μ_0 is the standard state chemical potential, R the gas constant, $H^* = H^*_0 e^{-\frac{\mu_0}{RT}}$ the intrinsic water solubility (H^*_0 is a constant; see *Richard et al.* [2006] for details) and κ_H the water diffusivity, which is assumed to be constant (see section 3.3). The influence of temperature-dependent

Table 1. Variables and Parameters Used in This Paper

Symbols	Names	Values	Units
	Parameters		
R	Gas constant	8.314	J mol^{-1} K^{-1}
κ	Thermal diffusivity	10^{-6}	m^2 s^{-1}
k_H	Water diffusivity	10^{-7}–10^{-11a}	m^2.s^{-1}
α	Thermal expansion coefficient	3–3.4×10^{-5b}	K^{-1}
β	Density water dependence coefficient	10^{-2} to 5×10^{-2c}	wt % H$_2$O^{-1}
T_0	Reference temperature (slab)	1150	°C
δT	Temperature range (slab-mantle)	300	°C
ρ_0	Reference mantle density (wadsleyite)	3500^c	kg m^3
η_0	Reference slab viscosity	10^{-21}	Pa s
H_0	Initial water concentration	1–2	wt %
μ_0	Standard state chemical potential	−10	kJ mol^{-1}
E	Activation enthalpy	∼600^d	kJ mol^{-1}
E^*	Pseudo-activation enthalpy	23×10^{-3}	K^{-1}
r	Power of the viscosity water dependence	1^d	-
	Variables		
H	Water concentration	-	wt %
T	Temperature	-	°C
τ_c	Onset time of the instability	-	Ma

^{a}From *Hae et al.* [2006].
^{b}From *Inoue et al.* [2004].
^{c}From *Angel et al.* [2001] and *Inoue et al.* [1998].
^{d}From *Karato* [2006] and *Mei and Kohlstedt* [2000].

solubility on water distribution has been previously investigated in details [*Richard et al.*, 2006] and shown to be relatively weak.

[9] The deviatoric stress tensor is

$$\underline{\tau} = \eta(\nabla \mathbf{u} + \nabla \mathbf{u}^t) \qquad (5)$$

The density ρ and viscosity η depend on temperature and water concentration [*Karato*, 2006], while the remaining properties are assumed to be constant. Density is assumed to follow a linear equation of state:

$$\rho = \rho_0(1 - \alpha(T - T_0) - \beta H) \qquad (6)$$

where H is the water content (wt %), α is the thermal expansivity, T_0 is the reference temperature corresponding to the reference density ρ_0, and β is a coefficient expressing the linear dependency of the density on water content. To focus on the effect of water on viscosity, we assume a Newtonian rheology for the mantle and discard the pressure dependence since small-scale convection occurs over small pressure range (see section 3 for details). Moreover, for computational simplicity we use a linear exponential viscosity; the use of this so-called Frank-Kamenetskii approximation is inconsequential considering the uncertainties on rheological properties of wadsleyite (and ringwoodite). Thus the viscosity η is given by

$$\eta = f(T, H) = \eta_0 H^{-r} e^{-E^*(T - T_0)} \qquad (7)$$

where E^* is a variable proportional to the activation enthalpy, T_0 the reference temperature (taken to be the slab temperature) and r an experimentally determined parameter ($r \sim 1$ [*Karato*, 2006]). Values and units of the controlling parameters are summarized in Table 1, and their effects are discussed in section 3.

[10] The boundary conditions for the water equation are fixed at the top and bottom of the box to the mantle water concentration (10^{-3} wt % H$_2$O). For the momentum equation, boundary conditions are free slip at the top and bottom of the box. For the top boundary, this assumption is supported by the large drop (2 orders of magnitude or more) in viscosity depicted by available data (geoid, topography, etc.) inversion [*Panasyuk and Hager*, 2000] to be likely at 410 km depth discontinuity (experiments with different settings, including the full transition zone, suggest than the results are weakly dependent from the top boundary condition). At the bottom, a reflective boundary condition is assumed for velocities (only the upper half of the slab is modeled) implying that shear stresses in the horizontal midplan of the slab are zero. The temperature in the upper mantle (top boundary of the box) is fixed and the heat flux at the midslab depth (bottom boundary) is fixed to be zero. This thermal boundary condition is only physically true for purely diffusive processes and becomes approximate as soon as convection starts. Nevertheless, we are mainly concerned with the conditions for the onset of convection, for which we can use this approximate condition. For both velocity and temperature the boundary condition of the sides are reflective. We have chosen a large aspect ratio (1:5) to mitigate side effects. Tests have been done in larger boxes (1:10), which do not change the results analyzed in section 4.

[11] To solve for this system of equations, we employ computational techniques used by *Christensen and Harder* [1991] but in two dimensions. The main feature of this numerical treatment is to split the viscosity at each horizontal level into a mean part and a fluctuating part $\eta(x, z) = \overline{\eta}(z) + \widetilde{\eta}(x, z)$ and then use a hybrid spectral and finite difference method to solve for the momentum equation (equation (2)). The temperature (equation (3)) and water (equation (4)) transport equations are advanced in time by an alternate direction implicit (ADI) scheme over a regular grid using an upwind scheme for the advection term [*Douglas and Rachford*, 1956]. The mesh size is 1 km × 0.4 km (512 × 256 grid points). Our code has been bench

marked against previous 2-D temperature-dependent rheology convection codes [*Blankenbach et al.*, 1989].

3. Controlling Parameters

[12] The parameters involved in our model are summarized in Table 1. Unfortunately, their actual values are not well constrained for the transition zone environment. Consequently, we define a plausible range of parameter space to cover likely transition zone conditions.

3.1. Density

[13] The process that we wish to model can be posed as a Rayleigh-Taylor instability [*Turcotte and Schubert*, 2002; *Mikaelian*, 1982] for which the driving force is known to be the density gradient. As stated in equation (6), the density of wadsleyite is here assumed to be only temperature- and water-dependent. The temperature dependence of density is parameterized by the thermal expansion coefficient α which has been experimentally measured to be between 30×10^{-6} K^{-1} (wet) and 34×10^{-6} K^{-1} (dry) [*Inoue et al.*, 2004]. In our settings, water concentration remains low (≤ 1 wt %) compared to the saturation level (≈ 3 wt %); thus, we have performed experiments with $\alpha = 34 \times 10^{-6}$ K^{-1}. Moreover, the effect of changing the thermal expansion coefficient has been considered and appears to be negligible. For example, with $\alpha = 30 \times 10^{-6}$ K^{-1} the onset time τ_c (see section 4.1) is less than 1 Ma shorter (i.e., less that 10% shorter) than with $\alpha = 35 \times 10^{-6}$ K^{-1}.

[14] The water dependence of the density is similarly parameterized by constant β (see equation (6)). To our knowledge, β has not been explicitly measured for wadsleyite and ringwoodite but a first-order approximation can be extracted from published data [*Inoue et al.*, 1998; *Angel et al.*, 2001]. From Figure 6 of *Angel et al.* [2001], hydrous wadsleyite (saturated with a theoretical maximum water content of 3.3 wt % H_2O) density is inferred to be 3300 kg m^{-3} and dry wadsleyite to be 3475 kg m^{-3}. Likewise, density is 3475 and 3590 kg m^{-3} for hydrous (2.7 wt % H_2O) and dry ringwoodite, respectively. These density values imply that $\beta = 2.44 \times 10^{-2}$ wt % H_2O^{-1} for wadsleyite. A similar linear regression using [*Inoue et al.*, 1998] data for ringwoodite yields $\beta = 1.67 \times 10^{-2}$ wt % H_2O^{-1}. In addition, recent studies on olivine suggest that the volumetric expansion due to hydration is significant. Under deep upper mantle conditions, the addition of 0.5 wt % H_2O to forsterite has the same effect on density as raising the temperature by about 240 K at zero pressure [*Smyth et al.*, 2006]. Because we use data from experiments not initially designed to estimate β, this parameter remains largely unconstrained. The amount of water (hydrogen) present in dry samples is for example unknown and assumed to be zero wt % H_2O and the amount of water present in saturated (wet) samples may not be the exact theoretical value. To fully account for these uncertainties, we employ a wide range for β from 1×10^{-2} to 5×10^{-2} wt % H_2O^{-1}.

3.2. Viscosity

[15] The mechanism underlying hydrolytic weakening in olivine is still under investigation [*Brodholt and Refson*, 2000], as it is in olivine high-pressure polymorphs (wadsleyite and ringwoodite). Nevertheless, transition zone minerals are commonly assumed to obey a power law rheology (dislocation creep); at high stress levels a flow law incorporating the effect of water [*Mei and Kohlstedt*, 2000; *Karato*, 2006] is given by

$$\dot{\varepsilon} = AH^r \exp\left(-\frac{E}{RT}\right)\sigma^n \tag{8}$$

where $\dot{\varepsilon}$ is the second invariant of strain rate (effective strain rate), σ the second invariant of stress and A, r and n are experimentally determined constants.

[16] For the sake of simplicity and because we are focusing specifically on the effect of water, we have made several assumptions regarding the effective viscosity (equation (7)):

[17] 1. The activation enthalpy is assumed to be constant, $E = U + PV = $ const (where U is the activation energy and V the activation volume); i.e., we neglect its pressure (P) dependence. In fact the pressure dependence on (wet) wadsleyite viscosity is not well known but olivine data provides some insights [*Karato*, 2006]. For wet olivine, the variation of E induced by the gradient of pressure δP within a 50km layer at the top of the slab (our settings) is around 10% ($10\delta PV \approx U$). Also, for mantle above a stagnant slab the pressure and temperature effects on viscosity are similar; i.e., they both make viscosity increase with depth.
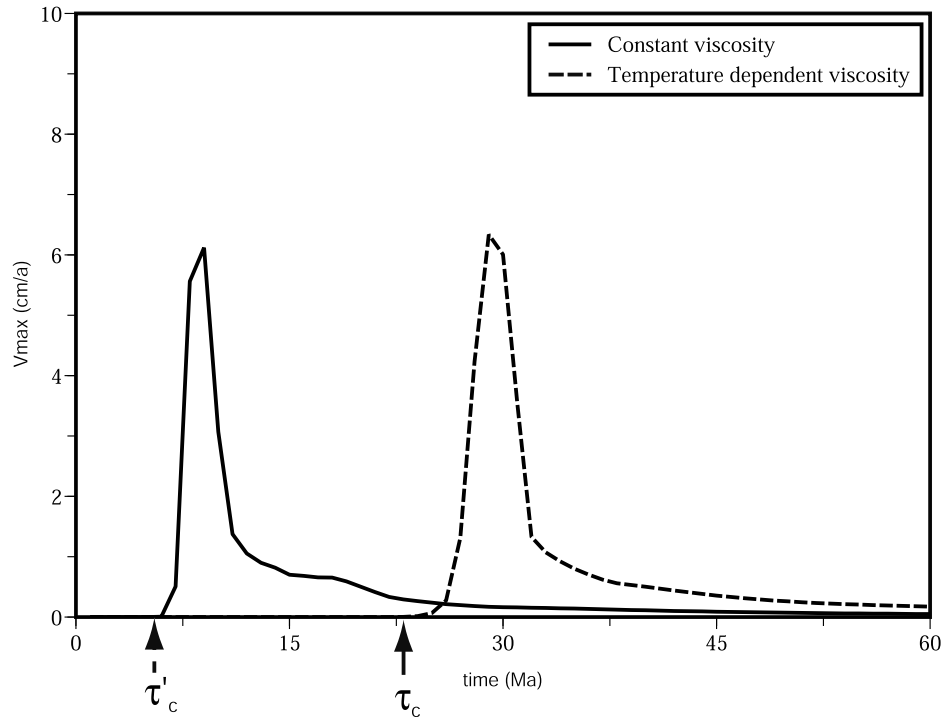
[18] The value of the enthalpy-related parameter $E^* = E/RT_0$ introduced in equation (7) has been chosen so that the initial ratio between the viscosity of the slab and the overlying mantle matches the "real" ratio (i.e., including pressure) inferred using the Arrhenius law (equation (8)) proposed for olivine by *Karato* [2006]. This ratio is close to one thousand, implying a 3 orders of magnitude variation of the viscosity due essentially to temperature. The measured value of r is close enough to the unity [*Mei and Kohlstedt*, 2000; *Karato*, 2006] to consider that the water dependence is linear.

[19] 2. The rheology is assumed to be Newtonian, such that $n = 1$. This assumption is commonly made in the study of small-scale sublithospheric convection (e.g., *van Hunen et al.* [2003]), which is a problem similar to ours. The geometry of our model, a 2-D coordinate system in the plane perpendicular to but following the slab-driven flow, is such that we focus on the formation of potential longitudinal rolls and assume that the shear stress in the direction of the slab motion (y axis) is uniform. It means that in our model framework (xz plane) the non-Newtonian effects are only related to the x and z directions. They become important only after the onset of the instabilities and thus may be neglected when the onset time is the diagnostic of interest.

3.3. Water Diffusivity

[20] The diffusivity of water in wadsleyite has been investigated through high-pressure experiments in the 900–1200°C temperature range. *Hae et al.* [2006] have determined that average diffusivity of water (i.e., the hydrogen ion) is similar to the diffusivity of water in olivine and can be approximated by $\kappa_H = 9.6 \ 10^{-6} \exp(E_D/RT)$, where $E_D = -123(\pm 32)$ kJ mol^{-1}.

[21] In our model, we assume κ_H to be constant and explore the range of values suggested by the laboratory

Figure 2. Temporal evolution of the maximum velocity of the flow V_{max} for two types of viscosity. For constant viscosity, $\eta' = 10^{19}$ Pa s (solid line), and for a temperature-dependent viscosity, $\eta = 10^{21}e^{-E*(T-T_{slab})}$ Pa s (dashed line). Arrows display the onset times ($\tau_c' = 6.6$ Ma and $\tau_c = 25.2$ Ma) when V_{max} reach $V_c = 0.1$ cm a^{-1} (see section 4.1 for details). The effects of water on viscosity are not taken into account ($r = 0$), the dependency of density on water ($\beta = 5 \times 10^{-2}$ wt %$^{-1}$) and water diffusivity is set to $\kappa_H = 10^{-10}$ m^2 s^{-1}. Under these conditions, the triggering of instabilities in constant viscosity cases requires a very low viscosity ($\eta < 5 \ 10^{19}$ Pa s).

experiments. In fact results show that when κ_H is small compared to the temperature diffusivity (as in transition zone), the influence of temperature dependence of the water diffusivity on the onset of convection is negligible (see section 4.1). In our range of model temperatures, κ_H goes from 10^{-8} to 2×10^{-11} m^2 s^{-1}. As mentioned by *Hae et al.* [2006], experiments were conducted on silica in undersaturated conditions, thus results may be different from the real mantle where wadsleyite coexists with enstatite and garnet. To account for a possible increase of κ_H due to the presence of enstatite and garnet, we have chosen to slightly broaden the range of our study and thus we use $\kappa_H \in [10^{-7} \ 10^{-11}]$ m^2 s^{-1}.

4. Results

[22] Despite its complexity, the underlying physics of our system essentially relies upon the evolution of only two main variables: the water content H and the temperature T.
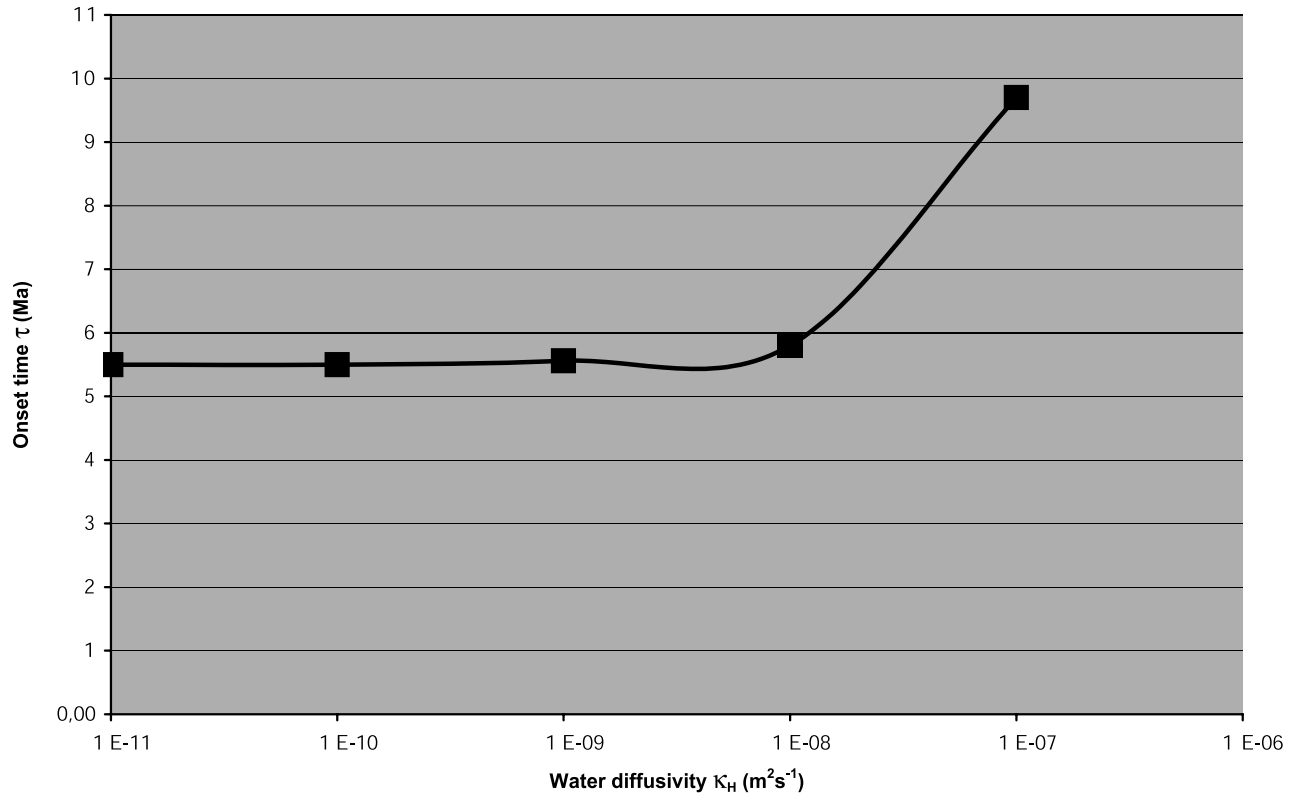
4.1. Onset Time of Stagnant Slab Water-Induced Convection

[23] Different criteria can be chosen to characterize the onset time of a gravitational instability τ_c. In studies on sublithospheric convection, temperature-based criteria are commonly used [*Davaille and Jaupart*, 1993; *Korenaga and Jordan*, 2003]. However, in our setting temperature is not the only controlling parameter, since the model does not treat a standard convection problem but instead concerns an episodic compositionally driven gravitational instability, thus a kinetic criterion (based on velocity) appears to be more suitable.

[24] The horizontal velocity of the slab V_y^{slab} is the zeroth order characteristic velocity of the system. Thus, we define τ_c as the time elapsed between the initiation of the slab's horizontal trajectory in the transition zone and the instant when the norm of the local convective velocity is somewhere larger than 1% of the horizontal slab velocity, $|V| = \sqrt{V_x^2 + V_z^2} > 0.01 \ V_y^{slab}$. The horizontal velocity of floating slabs is estimated to be of the order of $V_y^{slab} = 10$ cm a^{-1} [*DeMets et al.*, 1994] thus we have chosen 1 mm a^{-1} as a velocity threshold. On a plot of maximum velocity (within the xz plane) versus time (Figure 2), it is evident that τ_c corresponds to the time when the convective velocity undergoes a rapid transition. Figure 2 displays the characteristic behavior of the velocity field for two types of viscosity. Convective velocity slowly increases until the instability starts, then increases rapidly, and finally decreases when all the water has left the slab and there is no more driving force for the flow. It is also worth noting that to observe instabilities using constant viscosity, an unrealistically low viscosity ($\eta < 5 \times 10^{19}$ Pa s) has to be assumed.

[25] Because we focus on the effects related to water, in the rest of this study the rheological parameters controlling the temperature dependence are fixed ($\eta_0 = 10^{-21}$ Pa s, $E* = 23 \times 10^{-3}$ K^{-1}). The influence of water on onset time

Figure 3. Effect of the water diffusivity on the kinetic onset time of the gravitational instability. Time delay between the entry of the stagnant slab into the transition zone and the onset of the gravitational instability is displayed as a function of the water diffusivity κ_H. The other parameters are $(r, \beta$ wt %$^{-1}$, H_0 wt %) equal to $(1, 2.5 \times 10^{-2}, 1)$; τ_c decreases with decreasing water diffusivity and eventually reaches an asymptotic value. (See section 4.1 for details.)
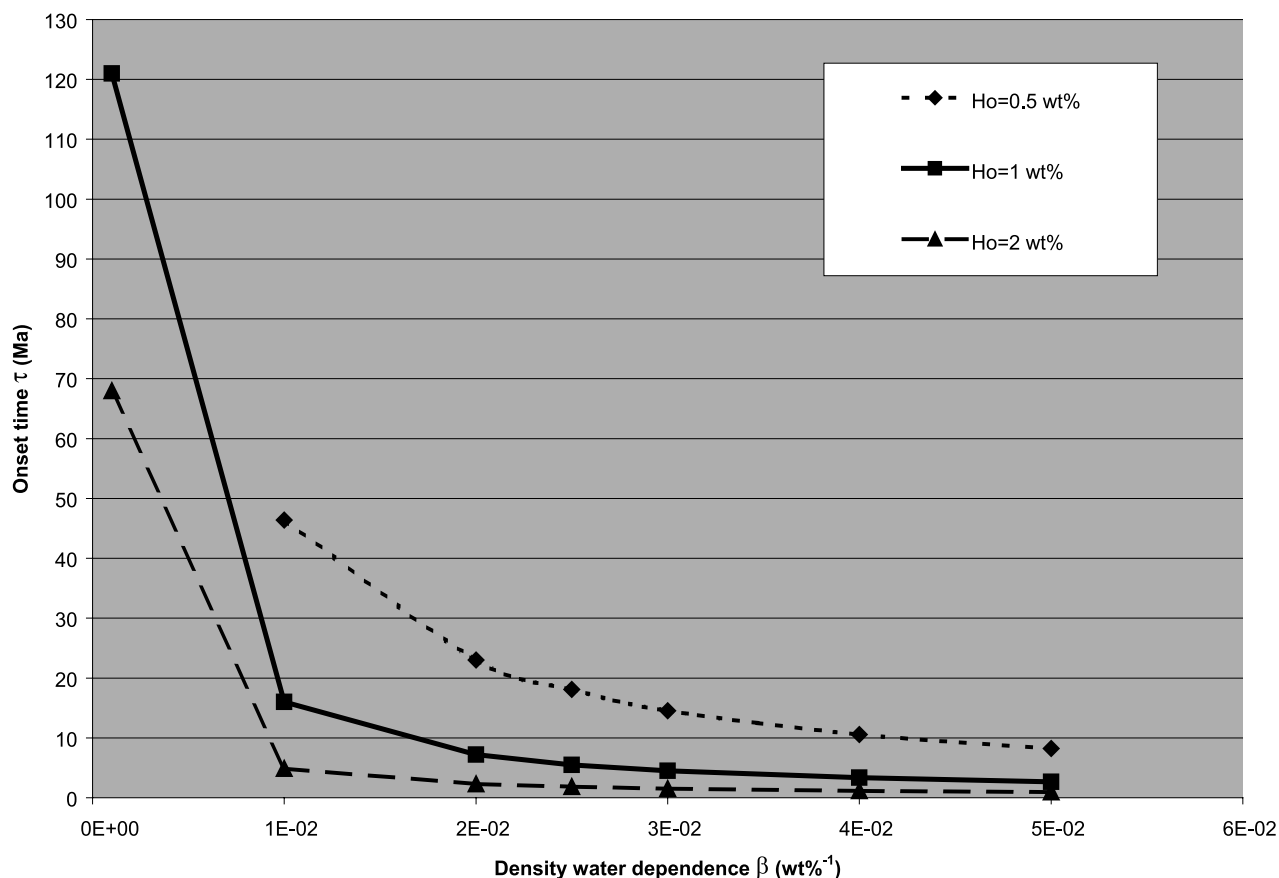
depends mainly on four parameters: (1) the initial water content of the slab H_0; (2) the water dependence of density β; (3) the water diffusivity κ_H; and (4) the water dependence of viscosity r. The onset time τ_c is plotted in Figure 3 as a function of κ_H and in Figure 4 as a function of β for H_0 in the 0.5–2 wt % range. The observed length of stagnant slabs in the transition zone rarely exceed 1000 km [*Fukao et al.*, 2001], which, assuming a slab velocity of 10 cm a^{-1}, corresponds to 100 Ma; thus, most of the numerical experiments presented here are stopped after that time interval. (Interestingly, longer runs indicate that after such a long time, triggering of diapirism is exceptional because water has had time to diffuse away from the top layer of the slab and the density contrast is largely erased.)

[26] For the most mantle-like set of parameters ($r = 1$, $H_0 = 1$ wt % $\beta = 2.5 \times 10^{-2}$ wt %$^{-1}$, $\eta_0 = 10^{-21}$ Pa s $E^* = 23 \times 10^{-3}$ K^{-1}, $\kappa_H = 10^{-10}$ m^2 s^{-1}), wet diapirs start to develop rapidly (after 5.5 Ma). Nevertheless, this value is β-dependent. Indeed, with a smaller value of $\beta = 10^{-3}$ wt %$^{-1}$ the onset time τ_c effectively increases to infinity ($\tau_c > 100$ Ma), thus precluding the occurrence of convective transport. In other words, there exists a certain threshold value of β under which the onset time τ_c is not a function of β anymore. This threshold, β_c, is essentially controlled by the amount of water available to decrease the density at the top of the slab (initial water content H_0). For our mantle-like set of parameters, β_c is just below 10^{-3} wt %$^{-1}$, at the lower

end of the range of realistic values. For high initial water content ($H_0 = 2$ wt %) the diapirs are likely to rise rapidly in all cases ($\beta_c \ll 1$), which has important implications on the water and temperature distribution (see section 4.2). For low initial water content ($H_0 = 0.5$ wt %), β has to be larger than $\beta_c \approx 2 \times 10^{-2}$ wt %$^{-1}$ to keep τ_c shorter than the 100 Ma limit.

[27] As depicted in Figure 3, lower water diffusivity κ_H induces a smaller onset time τ_c as well as smaller β_c. The decrease of τ_c with decreasing κ_H also reaches an asymptotic value when κ_H becomes small (3 orders of magnitude and more) compared with the temperature diffusivity ($\kappa = 10^{-6}$ m^2 s^{-1}). This implies that when κ_H is small, τ_c increases linearly with decreasing water dependence of density β and increases exponentially with decreasing β for high value of $\kappa_H \approx 10^{-7}$ m^2 s^{-1}. According to the experimental data [*Hae et al.*, 2006], the variations of wadsleyite diffusivity due the temperature variation stay within this range ($\kappa_H \in (10^{-9}\ 10^{-11})$ m^2 s^{-1}), verifying our constant water diffusivity assumption.

[28] The control of the water dependence of viscosity on the onset time τ_c is also of importance. The water-dependent viscosity case ($r = 1$) and water-independent case ($r = 0$) will, all else being equal, exhibit large differences. Without hydrolytic weakening, wet diapirs need much more time to be triggered ($\tau_c = 43$ Ma). Moreover, if high water diffusivity ($\kappa_H > 10^{-8}$ m^2 s^{-1}) is assumed, they require a

Figure 4. Kinetic onset time of the gravitational instability. Time delay between the entry of the stagnant slab into the transition zone and the onset of the gravitational instability is displayed as a function of the water dependence of density (through the parameter β defined in equation (6)). Water diffusivity is set to $\kappa_H = 10^{-10}$ m^2 s^{-1}. As expected, τ_c decreases with increasing density water dependence (β) and with larger initial water content (H_0). (See section 4.1 for details).

strongly water-dependent density ($\beta \geq 10^{-1}$ wt%$^{-1}$) to occur and thus would be unlikely in the Earth's mantle.

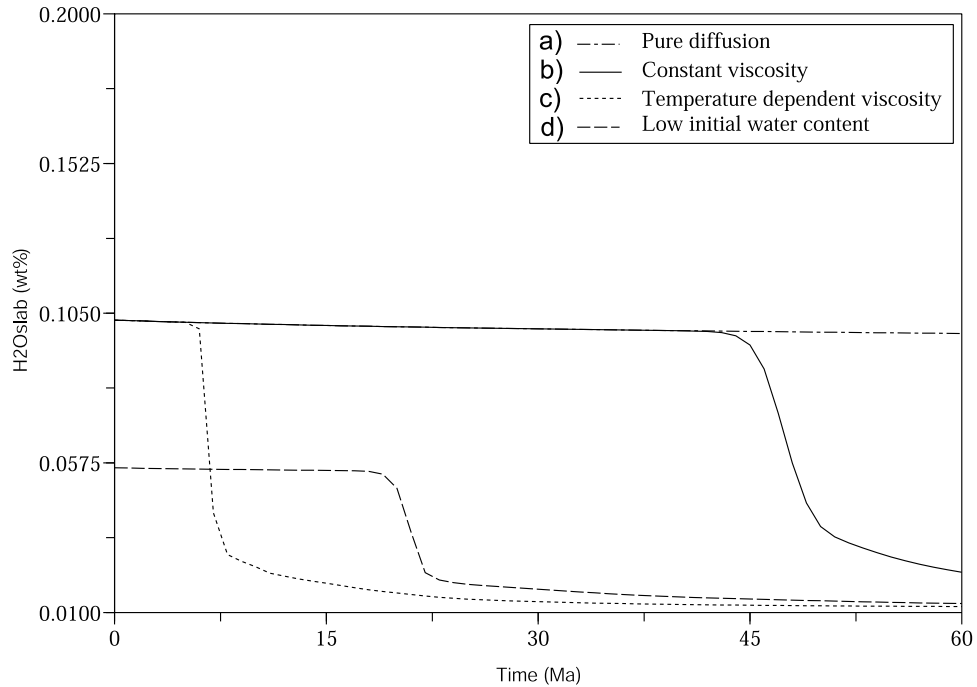## 4.2. Water Content and Temperature Temporal Evolution

[29] The temporal evolution of slab water content (Figure 5) displays three different types of dehydration processes: (1) Initially, there is a fast and short diffusion stage in which the initial sharp contrast in water between the slab and mantle smoothes slightly (barely discernible when water diffusivity is low ($\kappa_H < 10^{-8}$ m^2 s^{-1}). (2) This is followed by a slow diffusion stage in which the average amount of water in the slab slowly decreases as the slab water diffuses toward the dry mantle. (3) Last, water content undergoes an advective stage in which the diapiric instability develops and the rate of dehydration is accelerated. The average water concentration is reduced under the advective stage by at least a factor of 2 compared with a purely diffusive behavior. This diapiric instability recycles water into the mantle within a short time interval (5–15 Ma).

[30] Depending on the initial properties, the system is seen to follow two kinds of temporal evolution, going from one type of dehydration to the other. Purely diffusive sequences go from type 1 to type 2, and advective sequences go from type 1 to 2 to 3 and back to 2. For advective-
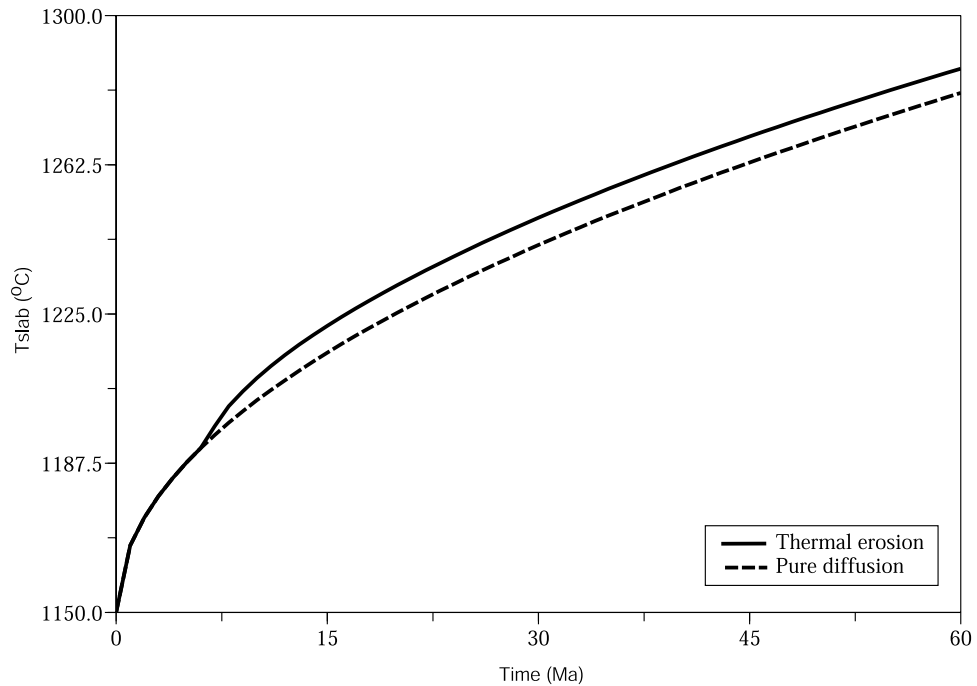
type evolution (see Figure 7 and the auxiliary material) (see the auxiliary material for a 2-D animation of water content, temperature and viscosity temporal evolution for realistic set of parameters $H_0 = 1$ wt %, $\beta = 2.5 \times 10^{-2}$ wt %$^{-1}$, $\kappa_H = 10^{-10}$ m^2 s^{-1} and $r = 1$), the final stage involves a return to a diffusive dehydration rate since there is insufficient water to drive the gravitational instability.[1] The effect of hydrolytic weakening is illustrated in Figure 5. With such weakening and an initial water concentration of $H_0 = 1$ wt % and $\beta = 2.5 \times 10^{-2}$ wt %$^{-1}$, diapiric instabilities recycle water into the mantle after 5.5 Ma (i.e., undergo rapid shift from type 2 to type 3). Without hydrolytic weakening ($r = 0$) instabilities are delayed (onset after 43 Ma). They are even prevented from developing if the water diffusivity is assumed to be high compared to the best fit value ($\kappa_H > 10^{-8}$ m^2 s^{-1}). In this case, there is only diffusive transport.

[31] For a realistic set of parameters ($r = 1$, $H_0 = 1$ wt % and $\beta = 2.5 \, 10^{-2}$ wt %$^{-1}$, $\kappa_H = 10^{-10}$ m^2 s^{-1}) the maximum flow velocity associated with water-induced gravitational instabilities is a few centimeters per year, up to 22 cm a^{-1} at the onset of convection (the evolution of the maximum velocity is displayed in Figure 2). This advective velocity is
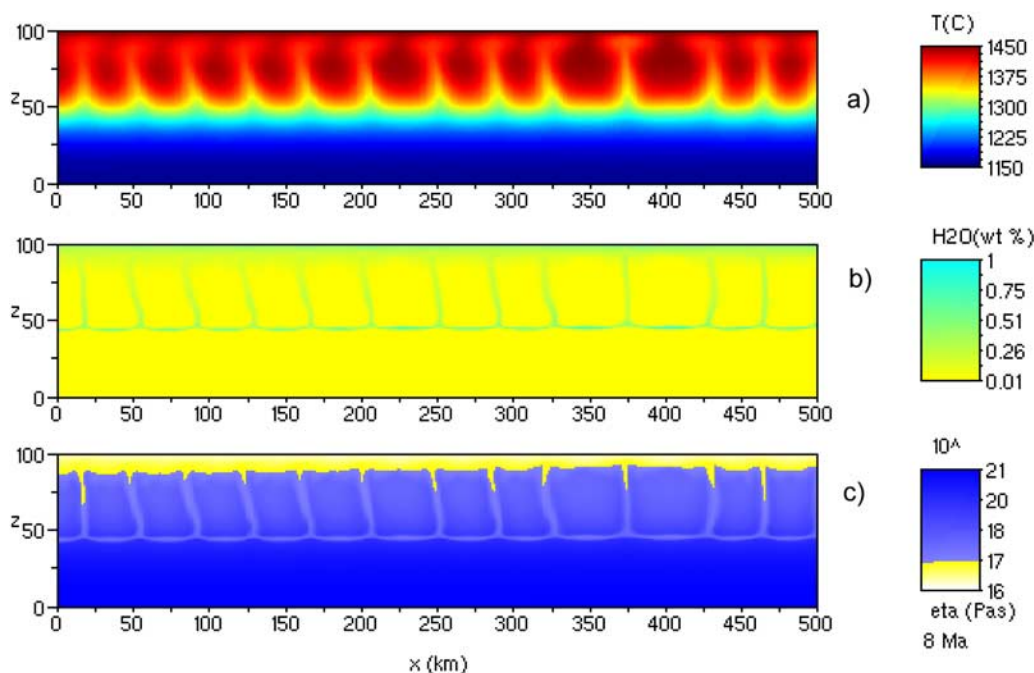
---

[1]Auxiliary materials are available in the HTML. doi:10.1029/2008JB005734.

Figure 5. Temporal evolution of slab water content. Average water content inside the slab is displayed for characteristic behaviors of the system. The cases a, b, c, d correspond to the sets of parameters (r, β wt %$^{-1}$, H_0 wt %, κ_H m^2 s^{-1}) equal to (0, 2.5 × 10^{-2}, 1, 10^{-10}) and constant viscosity ($\eta = 10^{21}$ Pa s), (0, 2.5 × 10^{-2}, 1, 10^{-10}), (1, 2.5 × 10^{-2}, 1, 10^{-10}), (1, 2.5 × 10^{-2}, 0.5, 10^{-10}), respectively. After a decrease reflecting the change from the initial step function distribution to the diffusive profile, water content is shown to first slowly decrease with time due to diffusion of water into the above dry mantle, then to drastically decrease (by approximately a factor of 2) if a convective episode takes place (cases b, c, d). (See section 4.2 for more details.)

Figure 6. Temporal evolution of slab temperature. Average temperature inside the slab is displayed. If a convective episode takes place, the slab is thermally eroded, and its averaged temperature (solid line) departs from the profile expected in a purely diffusive warming process (dashed line). Set of parameters used is $r = 1$, $\beta = 2.5 \times 10^{-2}$ wt %$^{-1}$ $H_0 = 1$ wt % $\kappa_H = 10^{-10}$ m^2 s^{-1} with a constant viscosity ($\eta = 10^{21}$ Pa s) in the pure diffusion case. (See section 4.2 and Table 1 for details.)

Figure 7. Snapshot of fully developed instabilities at the top of a stagnant slab. A mantle-like set of parameters, $r = 1$, $H_0 = 1$ wt %, $\beta = 2.5 \times 10^{-2}$ wt %$^{-1}$, $\eta_0 = 10^{-21}$ Pa s, $E^* = 23. \times 10^{-3}$ K^{-1}, $\kappa_H = 10^{-10}$ m^2 s^{-1}, is used, and snapshots are taken at the end of the advecting stage (3) described in section 4.2 (time $t = 8$ Ma, which is 2.5 Ma after the onset of convection). (a) Temperature field in degrees Celsius. (b) Water concentration in wt%H$_2$O. (c) Viscosity field in pascals per second. The horizontal wavelength of the instabilities is 25 km and mainly controlled by the viscosity of reference η_0. In later stages a secondary weaker convection cycle of the same wavelength is seen to develop (11 Ma) (see animations in the auxiliary material), and then both temperature and water concentration patterns are fading by diffusion.

similar to the large-scale convective flow ($\sim 2-10$ cm a^{-1}) and contributes to the transport of heat into the slab. The average temperature of the slab, which slowly increases with time when diffusion is the only transport process, is seen to encounter a sudden increase when instabilities develop (Figure 6). However, experimental results (see Figure 7 and the auxiliary material) reveal that the advective transport does not penetrate deep inside the slab because its viscosity is too high. Transport of heat into the slab is still essentially via diffusion, but the diffusive boundary layer is thinned by the small-scale water-induced convection. In fact, the resulting temperature profile above the slab is associated with the thermal erosion process as can occur at the base of the lithosphere [*Spohn and Schubert*, 1982; *Olson et al.*, 1988; *Monnereau et al.*, 1993].

5. Concluding Remarks

[32] Because foundering slabs in the transition zone are heated from above, small-scale thermal convection is impossible, but the presence of water in the slab can trigger Rayleigh-Taylor type instabilities of the top of the slab. The influence of water depends on four factors that are (1) the water dependence of density, (2) the initial amount of water present in the slab when it starts to linger in the transition zone, (3) the water diffusivity, and (4) the water dependence of viscosity.

[33] The effects of dissolved water within the principal transition zone minerals (wadsleyite and ringwoodite) are still not well constrained. To our knowledge no systematic measurements have been made to characterize their density as a function of water content. We can estimate this effect by considering data from studies on other material properties [*Angel et al.*, 2001; *Inoue et al.*, 1998] (see section 3.1), which suggest $\beta \approx 1-3 \times 10^{-2}$ wt %$^{-1}$. In this range, a water-dependent viscosity (from hydrolytic weakening), an average water diffusivity ($\kappa_H = 10^{-10}$ m^2 s^{-1}) and plausible water content ($H_0 \geq 0.5$ wt %) are necessary for gravitational instabilities to develop.

[34] Two assumptions inherent to our model are worthwhile to discuss. First, we have assumed that the concentration of water and the temperature field were initially (at the entry of the slab in the transition) constant along the direction perpendicular to the slab. Consequently, the quantitative values of the onset time produced by our model (see section 4.1) are an upper bound to the expected natural values. Second, we have restricted our model to the upper half of the slab, assuming a reflective lower boundary condition to focus on the effects related to the presence of water. In fact, experiments including the entire slab display almost no difference regarding the onset time and geometry (wavelength of the convective cells) of water-induced convection but a second episode of regular thermal convection (heating from below) is seen to initiate from the warm mantle layer below the slab (with a 10 times longer

wavelength assuming our preferred mantle like set of parameters).

[35] When water-induced gravitational instabilities take place, the consequences are twofold. First, this phenomenon facilitates the slab dehydration process (by a factor of 2 or more), and second, it enhances slab heating. For the sake of clarity, we have considered that the slab and mantle are composed of the same mineral (wadsleyite) discarding all the petrological heterogeneity due to the oceanic crust. Nevertheless, it is interesting to note that floating slabs are essentially old and cold material [*Fukao et al.*, 2001] that are expected to preserve relatively large amounts of water down to this depth [*Komabayashi et al.*, 2004; *Ruepke et al.*, 2004], making the phenomenon described here a common occurrence in the Earth's mantle; This implies that the transition zone overlying these slabs is probably hydrated as suggested by electrical conductivity data [*Ichiki et al.*, 2006]. A relatively wet or damp transition zone is a necessary condition for the formation of a 410 km depth "water filter" melt layer [*Bercovici and Karato*, 2003; *Karato et al.*, 2006] and the convective dehydration of floating slabs could explain the recently reported observations of melt at the top of southern California transition zone [*Toffelmier and Tyburczy*, 2007].

[36] To constrain our model seismic studies of the top of stagnant slab are insightful. They would give us information on the thermal state of the mantle overlying a stagnant and possibly detect the predicted "hydrous plumes." Unfortunately, they are usually focusing on along slab variation and not on slices perpendicular to the slab motion that are of interest for us. The temperature of the slab is also influenced by the episode of water-induced convection, through thermal erosion. Water-induced convection is likely to induce a sudden increase in slab temperature (relative to slab heating by diffusion alone), which induces a decrease in the average slab density. The dynamics of the slab should be affected by this density drop and thus our model suggests that once the slabs linger, the length of their stay in the transition zone is strongly water-dependent. Further consequences on the large-scale dynamical behavior of slabs are still to be investigated but our model suggests that water is playing a key role.

References

Angel, R. J., D. J. Frost, N. L. Ross, and R. Hemley (2001), Stabilities and equations of state of dense hydrous magnesium silicates, *Phys. Earth Planet. Inter.*, *127*, 181–196.

Bell, D., and G. Rossman (1992), Water in the Earth's mantle: The role of nominally anhydrous minerals, *Science*, *255*, 1391–1397.

Bercovici, D., and S.-I. Karato (2003), Whole-mantle convection and the transition-zone water filter, *Nature*, *425*, 39–43.

Blankenbach, B., et al. (1989), A benchmark comparison for mantle convection codes, *Geophys. J. Int.*, *98*(1), 23–38.

Brodholt, J., and K. Refson (2000), An ab initio study of hydrogen in forsterite and a possible mechanism for hydrolytic weakening, *J. Geophys. Res.*, *105*, 18,977–18,982.

Christensen, U., and H. Harder (1991), 3-d convection with variable viscosity, *Geophysic. J. Int.*, *104*(1), 213–220.

Davaille, A., and C. Jaupart (1993), Transient high Rayleigh number thermal convection with large viscosity variations, *J. Fluid Mech.*, *253*, 141–166.

DeMets, C., R. G. Gordon, D. F. Argus, and S. Stein (1994), Effect of recent revisions to the geomagnetic reversal time scale on estimates of current plate motions, *Geophys. Res. Lett.*, *21*, 2191–2194.

Douglas, J., and G. Rachford (1956), On the numerical solution of heat conduction problems in two and three space variables, *Trans. Am. Math. Soc.*, *82*, 421–439.

Fukao, Y., S. Widiyantoro, and M. Obayashi (2001), Stagnant slabs in the upper and lower mantle transition region, *Rev. Geophys.*, *39*, 291–324.

Gerya, T., and D. Yuen (2003), Rayleigh-taylor instabilities from hydration and melting propel 'cold plumes' at subduction zones, *Earth Planet. Sci. Lett.*, *212*, 47–62.

Hae, R., E. Ohtani, T. Kubo, T. Koyama, and H. Utada (2006), Hydrogen diffusivity in wadsleyite and water distribution in the mantle transition zone, *Earth Planet. Sci. Lett.*, *243*, 141–148.

Hirth, G., and D. Kohlstedt (1996), Water in the oceanic upper mantle: Implications for rheology, melt extraction and the evolution of the lithosphere, *Earth Planet. Sci. Lett.*, *144*, 93–108.

Ichiki, M., K. Baba, M. Obayashi, and H. Utada (2006), Water content and geotherm in the upper mantle above the stagnant slab: Interpretation of electrical conductivity and seismic P-wave velocity models, *Phys. Earth Planet. Inter.*, *155*, 1–15, doi:10.1016/j.pepi.2005.09.010.

Inoue, T., D. J. Weidner, P. A. Northrup, and J. B. Parise (1998), Elastic properties of hydrous ringwoodite (γ-phase) in $Mg_2 SiO_4$, *Earth Planet. Sci. Lett.*, *160*, 107–113.

Inoue, T., Y. Tanimoto, T. Irifune, T. Suzuki, H. Fukui, and O. Ohtaka (2004), Thermal expansion of wadsleyite, ringwoodite, hydrous wadsleyite and hydrous ringwoodite, *Phys. Earth Planet. Inter.*, *143–144*, 279–290.

Jacobsen, S., and S. van der Lee (Eds.) (2006), *Earth's Deep Water Cycle*, *Geophys. Monogr. Ser.*, vol. 168, AGU, Washington, D. C.

Karato, S.-I. (2006), Influence of hydrogen-related defects on the electrical conductivity and plastic deformation of mantle minerals: A critical review, in *Earth's Deep Water Cycle*, *Geophys. Monogr. Ser.*, vol. 168, edited by S. Jacobsen and S. van der Lee, pp. 113–129, AGU, Washington, D. C.

Karato, S.-I., D. Bercovici, G. Leahy, G. Richard, and Z. Jing (2006), Transition zone water filter model for global material circulation: Where do we stand?, in *Earth's Deep Water Cycle*, *Geophys. Monogr. Ser.*, vol. 168, edited by S. Jacobsen and S. van der Lee, pp. 70–89, AGU, Washington, D. C.

Kohlstedt, D., H. Keppler, and D. Rubie (1996), Solubility of water in the alpha, beta and gamma phases of (Mg,Fe) (2)sio₄, *Contrib. Mineral. Petrol.*, *123*(4), 345–357.

Komabayashi, T., S. Omori, and S. Maruyama (2004), Petrogenetic grid in the system $MgO-SiO_2-H_2O$ up to 30 GPa, 1600°C: Applications to hydrous peridotite subducting into the Earth's deep interior, *J. Geophys. Res.*, *109*, B03206, doi:10.1029/2003JB002651.

Komabayashi, T., K. Hirose, K.-I. Funakoshi, and N. Takafuji (2005), Stability of phase a in antigorite (serpentine) composition determined by in situ x-ray pressure observations, *Phys. Earth Planet. Inter.*, *151*, 276–289.

Korenaga, J., and T. H. Jordan (2003), Physics of multiscale convection in Earth's mantle: Onset of sublithospheric convection, *J. Geophys. Res.*, *108*(B7), 2333, doi:10.1029/2002JB001760.

Leahy, G. M., and D. Bercovici (2007), On the dynamics of a hydrous melt layer above the transition zone, *J. Geophys. Res.*, *112*, B07401, doi:10.1029/2006JB004631.

Mei, S., and D. Kohlstedt (2000), Influence of water on plastic deformation of olivine aggregates: 2. Dislocation creep regime, *J. Geophys. Res.*, *105*, 21,471–21,482.

Mikaelian, K. (1982), Rayleigh-taylor instabilities in stratified fluids, *Phys. Rev. A*, *26*(4), 2140–2158.

Monnereau, M., M. Rabinowicz, and E. Arquis (1993), Mechanical erosion and reheating of the lithosphere: A numerical model for hotspot swells, *J. Geophys. Res.*, *98*, 809–823.

Ohtani, E., K. Litasov, T. Hosoya, T. Kubo, and T. Kondo (2004), Water transport into the deep mantle and formation of a hydrous transition zone, *Phys. Earth Planet. Int.*, *143–144*, 255–269.

Olson, P., G. Schubert, C. Anderson, and P. Goldman (1988), Plume formation and lithosphere erosion - A comparison of laboratory and numerical experiments, *J. Geophys. Res.*, *93*, 15065–15084.

Panasyuk, S. V., and B. H. Hager (2000), Inversion for mantle viscosity profiles constrained by dynamic topography and the geoid, and their estimated errors, *Geophys. J. Int.*, *143*(3), 821–836.

Richard, G., M. Monnereau, and J. Ingrin (2002), Is the transition zone an empty water reservoir-Inferences from numerical model of mantle dynamics, *Earth Planet. Sci. Lett.*, *205*, 37–51.

Richard, G., D. Bercovici, and S.-I. Karato (2006), Slab dehydration in the Earth's mantle transition zone, *Earth Planet. Sci. Lett.*, *251*, 156–167.

Richard, G., M. Monnereau, and M. Rabinowicz (2007), Slab dehydration and fluid migration at the base of the upper mantle: Implications for deep earthquake mechanisms, *Geophys. J. Int.*, *168*, 1291–1304.

Richter, F., and B. Parsons (1975), On the interaction of two scales of convection in the mantle, *J. Geophys. Res.*, *80*, 2529–2541.

Ruepke, L., J. Phipps-Morgan, M. Hort, and J. Connolly (2004), Serpentine and the subdcution zone water cycle, *Earth Planet Sci. Lett.*, *223*, 17–34.

Schmeling, H. (1989), Compressible convection with constant and variable viscosity: The effect on slab formation, geoid, and topography, *J. Geophys. Res.*, *94*, 12,463–12,481.

Schmidt, M., and S. Poli (1998), Experimentally based water budgets for dehydrating slab and consequences for arc magma generation, *Earth Planet Sci. Lett.*, *163*, 361–379.

Smyth, J. R., D. J. Frost, F. Nestola, C. M. Holl, and G. Bromiley (2006), Olivine hydration in the deep upper mantle: Effects of temperature and silica activity, *Geophys. Res. Lett.*, *33*, L15301, doi:10.1029/2006GL026194.

Solomatov, S. V., and A. C. Barr (2007), Onset of convection in fluids with strongly temperature-dependent, power-law viscosity: 2. Dependence on the initial perturbation, *Phys. Earth Planet. Inter.*, *165*, 140–145, doi:10.1016/j.pepi.2005.11.001.

Spohn, T., and G. Schubert (1982), Convective thinning of the lithosphere: A mechanism for the initiation of continental rifting, *J. Geophys. Res.*, *87*, 4669–4681.

Thompson, A. (1992), Water in the Earth's mantle, *Nature*, *358*, 295–302.

Toffelmier, D., and J. Tyburczy (2007), Electromagnetic detection of a 410-km-deep melt layer in the southwestern united states, *Nature*, *447*, 992–994.

Turcotte, D., and G. Schubert (2002), *Geodynamics*, 2nd ed., Cambridge Univ. Press, Cambridge, U.K.

van Hunen, J., J. Huang, and S. Zhong (2003), The effect of shearing on the onset and vigor of small-scale convection in a Newtonian rheology, *Geophys. Res. Lett.*, *30*(19), 1991, doi:10.1029/2003GL018101.

Zhao, D. (2004), Global tomographic images of mantle plumes and subducting slabs: Insight into deep Earth dynamics, *Phys. Earth Planet. Inter.*, *146*, 3–34, doi:10.1016/j.pepi.2003.07.032.

————————————

G. C. Richard, Institut fuer Geowissenschaften, Facheinheit Geophysik, J. W. Goethe-Universitaet Frankfurt am Main, Altenhoeferallee 1, D-60438 Frankfurt am Main, Germany. (richard@geophysik.uni-frankfurt.de)

D. Bercovici, Department of Geology and Geophysics, Yale University, P.O. Box 208109, New Haven, CT 06520-8109, USA.